The Astrophysical Journal, 902:106 (12pp), 2020 October 20 https://doi.org/10.3847/1538-4357/abb40b

The Elusive Distance Gradient in the Ultrafaint Dwarf Galaxy Hercules: A Combined Hubble Space Telescope and Gaia View

Burçin Mutlu-Pakdil[1,2,3], David J. Sand[1], Denija Crnojević[4], Edward W. Olszewski[1], Dennis Zaritsky[1], Jay Strader[5], Michelle L. Collins[6], Anil C. Seth[7], and Beth Willman[8]
[1] Department of Astronomy/Steward Observatory, 933 North Cherry Avenue, Rm. N204, Tucson, AZ 85721-0065, USA; burcinmp@uchicago.edu
[2] Kavli Institute for Cosmological Physics, University of Chicago, Chicago, IL 60637, USA
[3] Department of Astronomy and Astrophysics, University of Chicago, Chicago, IL 60637, USA
[4] University of Tampa, 401 West Kennedy Boulevard, Tampa, FL 33606, USA
[5] Department of Physics and Astronomy, Michigan State University, East Lansing, MI 48824, USA
[6] Department of Physics, University of Surrey, Guildford GU2 7XH, UK
[7] University of Utah, 115 South 1400 East, Salt Lake City, UT 84112-0830, USA
[8] LSST and Steward Observatory, 933 North Cherry Avenue, Tucson, AZ 85721, USA
Received 2020 July 22; revised 2020 August 24; accepted 2020 August 25; published 2020 October 16

Abstract

The ultrafaint dwarf galaxy Hercules has an extremely elongated morphology with both photometric overdensities and kinematic members at large radii, suggesting that it may be tidally disrupting due to a previous close encounter with the Milky Way. To explain its observational peculiarities, we present a deep Hubble Space Telescope (HST) imaging study of Hercules and its surrounding regions and investigate its tidal history through a careful search for a distance gradient along its stretched body. Our off-center HST data clearly resolve a main sequence, showing that the stellar extension seen along the major axis of Hercules is genuine, not a clump of background galaxies. Utilizing Gaia DR2 data, we clean the region around the Hercules of field contamination, and find four new plausible member stars, all of which are located on the outskirts of the dwarf galaxy. We update the distance to Hercules, and find 130.6 $\pm$ 6.1 kpc ($m - M = 20.58 \pm 0.10$) for the main body, which is consistent with earlier estimates in the literature. While we find no conclusive evidence for a distance gradient, our work demonstrates that constraining a distance gradient in such a faint system is not trivial, and the possible thickness of the dwarf along the line of sight and field contamination make it harder to make decisive conclusions even with these high-precision data. Future studies coupled with tailored theoretical models are needed to understand the true nature of Hercules and of tidal distortion observables in ultrafaint galaxies in general.

Unified Astronomy Thesaurus concepts: Dwarf galaxies (416); Galaxy interactions (600); Galaxy kinematics (602); Galaxy dynamics (591); Local Group (929); HST photometry (756); Proper motions (1295)

Supporting material: machine-readable tables

1. Introduction

Ultrafaint dwarf galaxies (UFDs, $M_V \gtrsim -7$) represent the extreme end of the distribution of galaxy properties: the least luminous, least chemically enriched, and most dark-matter-dominated galaxies known. These systems offer a unique avenue to study the cosmological nature of dark matter and galaxy formation on the smallest scales (for a recent review, see Bullock & Boylan-Kolchin 2017; Simon 2019).

In recent years, deep wide-area photometric surveys have greatly increased the known population of Milky Way satellites (e.g., Belokurov et al. 2008; Belokurov et al. 2009, 2010; Bechtol et al. 2015; Drlica-Wagner et al. 2015, 2016; Kim & Jerjen 2015; Kim et al. 2015; Koposov et al. 2015, 2018; Laevens et al. 2015a, 2015b; Martin et al. 2015; Homma et al. 2016, 2018; Torrealba et al. 2016; Mau et al. 2020). Following their discovery, the first important step is to constrain their dynamical masses and dark matter content via their stellar velocity dispersions, but this heavily relies on the assumptions of dynamical equilibrium. Yet, both spectroscopic and deeper photometric follow-up studies have uncovered signs of tidal interaction in several new ultrafaint systems (e.g., Simon & Geha 2007; Martin et al. 2008; Okamoto et al. 2008; Sand et al. 2009, 2012; Muñoz et al. 2010; Kirby et al. 2013; Carlin & Sand 2018; Erkal et al. 2018; Fritz et al. 2018; Li et al. 2018; Longeard et al. 2018; Muñoz et al. 2018; Mutlu-Pakdil et al. 2018; Shipp et al. 2018; Fu et al. 2019, among others). Therefore, in order to interpret them properly in a substructure formation context, it is crucial to determine whether UFDs are strongly affected by tidal forces. We recently addressed this fundamental question by presenting a comprehensive investigation of these signs of disruption in UFDs with a combined Hubble Space Telescope (HST), MMT/Hectochelle, and Gaia study of the distant Milky Way UFD Leo V (Mutlu-Pakdil et al. 2019). Our findings removed most of the observational clues that suggested Leo V was disrupting, highlighting the importance of deeper studies into the nature of UFDs. In this paper, we extend our investigation to Hercules—another strong candidate for a tidally disrupting UFD around the Milky Way—with a different strategy, where we search for a distance gradient along the stretched body of the galaxy.

There is observational evidence that Hercules might be undergoing tidal disruption by the Milky Way. It has an extreme ellipticity ($\epsilon \sim 0.7$, Coleman et al. 2007; Martin et al. 2008; Sand et al. 2009), making it the most elongated Milky Way satellite other than the disrupting Sagittarius dwarf (Ibata et al. 1994). Several photometric studies have found significant stellar overdensities far from its center (Sand et al. 2009; Roderick et al. 2015), and kinematics of a subset of member stars show velocity gradients (Adén et al. 2009; Deason et al. 2012). Additionally, Deason et al. (2012) found likely blue

horizontal branch (HB) members at large distances, and Garling et al. (2018) identified RR Lyrae members outside the nominal tidal radius.

Given the large distance of Hercules—one of the outermost known Milky Way satellites at $D \approx 130$ kpc—it can only experience tidal stripping if its orbit is extremely eccentric, bringing it within 10–20 kpc of the Galactic center (Fu et al. 2019; Simon 2019; Gregory et al. 2020). Such an orbit is plausible based on Gaia proper motions, which variously[9] predict a pericenter of 14^{+23}_{-9} kpc (or 20^{+32}_{-14} kpc), (Fritz et al. 2018); $47^{+27}_{-21.6}$ kpc, (Fu et al. 2019); or $50.9^{+24.2}_{-23.6}$ kpc, (Gregory et al. 2020). Note that Hercules seems to be rapidly moving away from the Milky Way at $v_{\rm GSR} \sim 145$ km s^{-1} (Simon & Geha 2007), but its orbital path is not well constrained with existing proper-motion data (Gregory et al. 2020).

Two compelling orbital models have been put forward to explain the observed peculiarities of Hercules. One is the Martin & Jin (2010) hypothesis in which Hercules is a segment of a tidal stream observed near apocenter, and its elongation is aligned with its orbital path. This model provides two strong testable predictions: there should be a substantial distance and velocity gradient along the major axis of Hercules. The other model is the Küpper et al. (2017) "exploding satellite" scenario where the disruption of the satellite is caused by a close pericenter passage ~0.5 Gyr ago. In this scenario, the stream in formation is actually aligned with the minor axis of Hercules. In this case, there should be tidal debris along the dwarf's minor axis and a distinct kinematic substructure, but the galaxy should not display any distance or velocity gradient along its extent. The positions of the substructures identified in Roderick et al. (2015) and distribution of RR Lyrae stars detected in Garling et al. (2018) are suggestive of an orbital path similar to this "exploding satellite" model.

Combining available kinematic data with proper motions from Gaia DR2, Fu et al. (2019) evaluated the probability that its orbit approaches sufficiently close to the Milky Way to experience tidal stripping, and found a probability of ~40% that Hercules has suffered tidal stripping. On the other hand, the authors were unable to confirm any members located in one of the most significant overdensities surrounding the galaxy that Roderick et al. (2015) identified ($\gtrsim 3r_h$ at the west side of Hercules; see Figure 2 of Fu et al. 2019). Recently, Gregory et al. (2020) used new spectroscopy from DEIMOS/Keck II, together with the Gaia DR2 data, and found no evidence for a significant velocity gradient or velocity substructure in their membership sample. They also noted, however, that their average velocity uncertainty per member star is comparable to the overall Hercules velocity dispersion, and therefore may blur out any residual velocity substructures. Additionally, the authors updated the systemic proper motion of Hercules, and found that the observed proper motion is slightly misaligned with the elongation of Hercules, in contrast to models that suggest that any tidal debris should be well aligned with the orbital path (e.g., Jin & Martin 2009; Martin & Jin 2010), but also inconsistent with the proper motion required for the "exploding satellite" scenario (Küpper et al. 2017). However, they argued that though the misalignment is not very significant, future observations from Gaia DR3, the Rubin Observatory, and the Roman Space Telescope may resolve this tension by providing significantly stronger constraints on the proper motion of Hercules. Fortunately, proper motion is not the only way to test the orbital models, and measurement of a distance gradient (or a lack thereof) across the body of Hercules may in fact be used to distinguish between these scenarios, and can serve as one of the most powerful probes for understanding the true nature of this object.

[9] Fritz et al. (2018) assumed a Milky Way dark matter halo with virial mass $1.6 \times 10^{12} M_\odot$ (or $0.8 \times 10^{12} M_\odot$). Both Fu et al. (2019) and Gregory et al. (2020) used a Milky Way virial mass $1.3 \times 10^{12} M_\odot$, but the latter also included the effect of the Large Magellanic Cloud and additional data points from new spectroscopy.

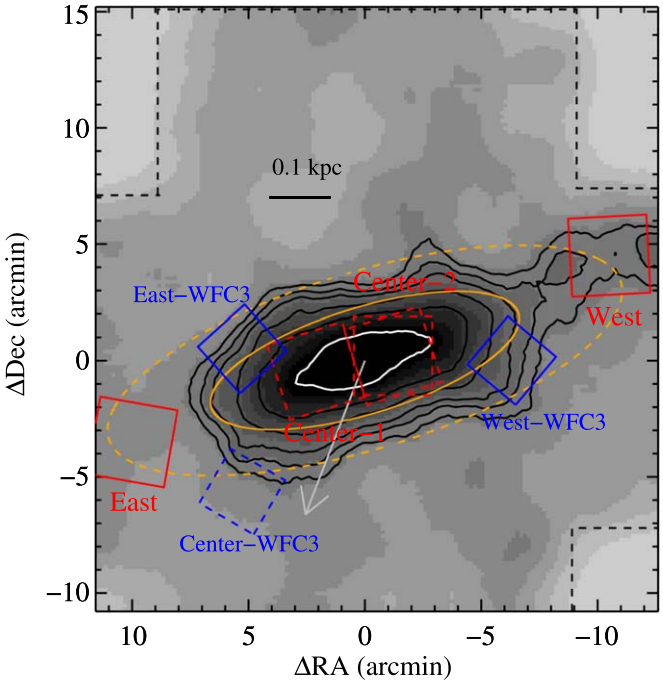

Figure 1. Our observing strategy: the smoothed matched-filter map of Hercules is derived from the ground-based Large Binocular Telescope (LBT) imaging of Sand et al. (2009), where the solid orange line marks the half-light radius (this value is comparable to the smoothing size). The dashed boxes represent the archived HST/ACS and WFC3 imaging that we utilized for our analysis. The solid boxes are our HST/ACS (red) observations along the major axis and the relative WFC3 (blue) parallel ones. The orange dashed ellipse is the approximate isodensity contour at the radius of our ACS data ($r \sim 2\times$ half-light radii). The gray arrow marks the weighted mean proper motion of Hercules (Gregory et al. 2020). The black dashed lines represent the actual LBT field of view.

In this work, we present a comprehensive deep HST imaging study of Hercules and its surrounding regions, combined with the Gaia DR2 archival data, and search for observational evidence of tidal disturbance in the form of a distance gradient. We describe our observations and data reduction in Section 2. We show its color–magnitude diagram (CMD) reaches well below the main sequence turnoff (MSTO) and compare it with that of M92 in Section 3. Using the Gaia DR2 data, we perform a membership analysis where we search for new Hercules member candidates while reducing the foreground contamination in Section 4. In Section 5, we revisit the distance to Hercules and explore the presence of a distance gradient across the galaxy. Finally, we summarize our key results in Section 6.

2. HST Imaging and Data Reduction

Deep optical observations along the major axis of Hercules were performed using the F606W and F814W filters on the Advanced Camera for Surveys (ACS) (HST-GO-15182; PI: D. Sand). Our observational strategy is outlined in Figure 1: the

Table 1
Observation Log and Field Completeness of Hercules

Field Name	Camera	Filter	Exp (s)	50% (mag)	90% (mag)
Center-1	ACS	F606W	12880	28.55	27.96
	ACS	F814W	12745	28.12	27.58
Center-2	ACS	F606W	12880	28.47	27.75
	ACS	F814W	12745	28.05	27.27
Center	WFC3	F606W	13635	28.17	27.15
	WFC3	F814W	13515	27.97	27.36
West	ACS	F606W	12726	28.15	27.14
	ACS	F814W	12726	27.90	27.34
	WFC3	F606W	12926	28.15	27.02
	WFC3	F814W	12926	27.91	27.36
East	ACS	F606W	13753	28.15	27.05
	ACS	F814W	21763[a]	27.99	27.08
	WFC3	F606W	12726	28.25	27.20
	WFC3	F814W	20848[a]	28.02	27.37

Notes. The Center-1/ACS, Center-2/ACS, and Center-WFC3 data are the available archival central fields of Hercules from HST-GO-12549 (Cycle 19, PI: T. Brown). The rest is our new HST observations from HST-GO-15182 (Cycle 25, PI: D. Sand), obtained with 10 orbits per field from 2018 March through 2020 February.
[a] Due to gyro issues, we had to repeat the observations of this field, which provided some extra data.

dashed boxes represent archived HST/ACS and Wide Field Camera 3 (WFC3) imaging, which we included in our analysis, and the solid boxes are our new observations. The $\sim 23'$ lever arm between our ACS pointings and the coordinated parallel observations with WFC3/UVIS were specifically designed to look for a predicted distance gradient across the galaxy. Table 1 presents the log of the observations. A standard four-point dither pattern was used to achieve 0.5 pixel sampling. The image depth was chosen to be consistent with the two available archival central pointings of Hercules from HST-GO-12549 (PI: T. Brown).

We performed point-spread function photometry on all of the new and archival HST data as described in Mutlu-Pakdil et al. (2019), which we briefly describe here. All photometry was performed on the flat-fielded (FLT) images using the latest version (2.0) of DOLPHOT (Dolphin 2002), an updated version of HSTPHOT (Dolphin 2000), largely using the recommended prescriptions on each camera. We used the synthetic Tiny Tim PSFs for all images. The catalogs were cleaned of background galaxies and stars with poor photometry, and we only included sources with $(\mathrm{sharpness}_{\mathrm{F606W}}+\mathrm{sharpness}_{\mathrm{F814W}})^2<0.1$, $(\mathrm{crowding}_{\mathrm{F606W}}+\mathrm{crowding}_{\mathrm{F814W}})<0.08$, signal-to-noise ratio >5, roundness <1.5, and object-type $\leqslant 2$ in each filter. We corrected for Milky Way extinction on a star-by-star basis using the Schlegel et al. (1998) reddening maps with the coefficients from Schlafly & Finkbeiner (2011). Table 2 presents our final catalogs, which include magnitudes (uncorrected for extinction) along with their DOLPHOT uncertainty, as well as the Galactic extinction values derived for each star. The extinction-corrected photometry is used throughout this work, and the CMDs are displayed in Figure 2. We derived completeness and photometric uncertainties using $\sim$50,000 artificial star tests per pointing (adding one artificial star at a time), with the same routines used to create the photometric catalogs. Note that there are $\sim$6000 stars in both our most populated central fields. The 50% completeness limit for F814W is $\sim$28 mag across all HST images (see Table 1).

3. Color–Magnitude Diagrams

Figure 2 presents the CMDs of our Hercules HST fields, the top panel for the ACS fields relative to the Galactic globular cluster M92[10]—one of the most ancient, metal-poor, and well-studied star clusters known—and the bottom panel for the WFC3 fields relative to the Hercules main body (i.e., Center-1 +Center-2). There are a number of studies devoted to Hercules (e.g., Coleman et al. 2007; Simon & Geha 2007; Kirby et al. 2008; Koch et al. 2008; Adén et al. 2009; Sand et al. 2009; Brown et al. 2014; Weisz et al. 2014), agreeing that Hercules is old (>12 Gyr, with negligible star formation in the last 12 Gyr) and very metal-poor (with values of the mean metallicity $\langle[\mathrm{Fe/H}]\rangle$ ranging from about -2.0 to -2.7 dex). In Figure 2, the CMDs of the central Hercules fields have well-defined features with a clear MSTO, displaying a close agreement with M92. A similarly close agreement with M92 was also found for Leo V (Mutlu-Pakdil et al. 2019), which suggests that M92 is a nice fit to UFD galaxies that are dominated by ancient metal-poor populations. Note that metallicity estimates for M92 range from $-2.4 < [\mathrm{Fe/H}] < -2.1$ (e.g., Sneden et al. 2000; Behr 2003; Carretta et al. 2009), while there is evidence for $[\mathrm{Fe/H}] < -2.5$ in individual M92 stars (e.g., Peterson et al. 1990; King et al. 1998; Roederer & Sneden 2011). Therefore, M92 provides an important empirical fiducial for the stellar populations of Hercules, which we will use to revisit its distance in Section 5.

The same central ACS fields were also studied by Brown et al. (2014), along with five other UFDs (i.e., Boötes I, Canes Venatici II, Coma Berenices, Leo V, and Ursa Major I). In addition to overall good agreement with M92, their CMDs show the presence of bluer and brighter stars near the MSTO when compared to the M92 ridgeline, hence the authors suggested the presence of a very metal-poor stellar population in these UFDs. However, as we addressed in Mutlu-Pakdil et al. (2019), the presence of a bluer and brighter star population in their CMDs can be explained with their adopted reddening values. Brown et al. (2014) derived the distance and extinctions from fits to the ACS data and adopted $E(B-V)=0.09$ mag for Hercules, which is higher than our adopted value ($E(B-V)=0.06$ mag on average, see Table 3), which comes from the Schlafly & Finkbeiner (2011) extinction derived from the Schlegel et al. (1998) reddening maps.

In the top panel of Figure 2, the CMDs of the off-center East and West ACS fields, both located at $\sim 2.5\times$ half-light radii (r_h), reveal a clear main sequence, suggesting the elongated nature of Hercules is indeed real and not clumps of compact background galaxies. We note that these stars still fall within $\sim 2.5 \times r_h$, hence they might be bound stars. The bottom panel compares the CMDs of our WFC3 fields, relative to the central ACS fields. Note that East- and West-WFC3 are at similar projected radii, e.g., their average projected distance along the photometric major axis (d) is $1\farcm2$ and $2\farcm0$, respectively, while Center-WFC3 and our off-center ACS fields are at comparable

[10] The details of the M92 HST photometry and our derivation of its fiducial sequence were described in Mutlu-Pakdil et al. (2019). Note that we implement the extinction correction for M92 using the same method described for Hercules, with an average $E(B-V)$ of 0.022 mag.

Table 2
Photometry of Hercules Fields

Field	Camera	Seq.	α (deg)	δ (deg)	F606W (mag)	δ(F606W) (mag)	A_{F606W} (mag)	F814W (mag)	δ(F814W) (mag)	A_{F814W} (mag)
Center-1	ACS	0	247.79626	12.788096	19.30	0.001	0.15	18.32	0.001	0.10
Center-1	ACS	1	247.79927	12.794552	19.22	0.001	0.15	18.30	0.001	0.09
Center-1	ACS	2	247.78386	12.801684	19.32	0.001	0.15	18.44	0.001	0.09
Center 2	ACS	0	247.72835	12.808475	19.54	0.001	0.15	18.56	0.001	0.09
Center 2	ACS	1	247.73296	12.791601	19.49	0.001	0.15	18.84	0.001	0.09
Center 2	ACS	2	247.73552	12.765498	20.67	0.001	0.16	18.43	0.002	0.10
Center	WFC3	0	247.85105	12.696190	19.47	0.001	0.16	18.29	0.001	0.10
Center	WFC3	1	247.87623	12.688866	20.64	0.001	0.16	18.68	0.001	0.10
Center	WFC3	2	247.84116	12.678297	20.06	0.001	0.16	19.28	0.001	0.10
West	ACS	0	247.60898	12.842439	19.34	0.000	0.15	18.54	0.000	0.09
West	ACS	1	247.58023	12.862125	19.45	0.000	0.15	18.72	0.000	0.09
West	ACS	2	247.56147	12.861518	19.57	0.001	0.15	18.75	0.001	0.09
West	WFC3	0	247.64271	12.794218	19.27	0.002	0.15	18.48	0.001	0.09
West	WFC3	1	247.66082	12.790000	19.80	0.001	0.15	18.15	0.001	0.09
West	WFC3	2	247.64324	12.805542	20.10	0.001	0.15	18.07	0.001	0.09
East	ACS	0	247.95740	12.720261	19.38	0.001	0.14	18.41	0.001	0.09
East	ACS	1	247.95326	12.750190	20.13	0.001	0.13	18.43	0.001	0.08
East	ACS	2	247.93314	12.744528	20.24	0.001	0.14	18.42	0.001	0.08
East	WFC3	0	247.83546	12.802458	19.28	0.002	0.15	18.38	0.000	0.09
East	WFC3	1	247.87718	12.804322	19.66	0.001	0.14	18.60	0.001	0.08
East	WFC3	2	247.87247	12.784672	19.31	0.002	0.14	18.83	0.001	0.09

(This table is available in its entirety in machine-readable form.)

projected radii (i.e., $d_{\mathrm{Center-WFC3}} = 7\farcm0$, $d_{\mathrm{East}} = 6\farcm4$, $d_{\mathrm{West}} = 7\farcm5$). In all of our off-center fields (i.e., East, West, Center/East/West-WFC3), the red giant branch (RGB) and subgiant branch (SGB) stars are not well populated, and the RGB suffers from significant field contamination, which is apparent from the scattering of stars beyond the M92 stellar locus. Although contamination includes unresolved background galaxies at magnitudes much fainter than the Hercules MSTO, it is dominated by Milky Way contaminants around the RGB. We will use the Gaia DR2 data to disentangle a significant fraction of Milky Way contaminants from Hercules members in Section 4. Furthermore, there is a number of stars spread around a color of ∼0.5 mag and between F814W ∼20.5 to ∼19 mag, extending above the HB level (especially, in Center-1, there almost seems to be a parallel RGB), and we will also investigate their membership with Gaia DR2 in the following section.

4. Membership Analysis

As shown in Figure 2, the outskirts of Hercules are poorly populated and heavily contaminated. Here, we review the known Hercules member and nonmember stars, and use Gaia DR2 to explore the membership of bright stars (F814W $<$ 20 mag) in our HST fields. Our aim is to search for further Hercules member candidates while reducing the foreground contamination, according to their proper motions. First, we compile a comprehensive set of Hercules members, using membership catalogs from Simon & Geha (2007), Adén et al. (2009), Deason et al. (2012), Musella et al. (2012), Garling et al. (2018), and Gregory et al. (2020). Then, we cross match our HST catalog to the Gaia DR2 archive, selecting only those stars with a match within 1″. This catalog matching returns a sample of 75 sources, of which 48 do not have any published spectroscopic data. The top left panel of Figure 3 shows the proper motions of all sources with a match in Gaia DR2. The known radial velocity members (red stars) form a tight distribution in proper-motion space, except for two with deviant proper motions—one (located in Center-1) comes from the Simon & Geha (2007) member catalog, and the other (located in West) comes from the Gregory et al. (2020) catalog. We classify these two stars as PM nonmembers (PM stands for proper motion). In Table 4, we present a clean members catalog for Hercules, after refining their membership using Gaia DR2 proper motions. Note that this catalog is based only on HST matches, so it does not extend beyond our HST footprint. As shown here (see also Simon 2018), the stars that have been spectroscopically classified as UFD member stars in the literature deserve a second look, as some of them might have Gaia proper motions very different from those of the galaxies that they supposedly belong to.

The top right panel of Figure 3 shows a close-up of the stars with acceptable proper motions, which we define as $|(\mu_\alpha \cos\delta, \mu_\delta)| \leqslant 2$ mas yr^{-1}. There are four new stars without spectroscopy but with a proper motion in this accepted range, and we label them as PM members in the figures and in Table 5. These stars are ideal targets for future spectroscopic studies of Hercules. We classify the rest of the stars without spectroscopy as PM nonmembers, as their proper motions imply that they are likely not a true Hercules member. The bottom panel of Figure 3 shows the spatial distribution of our new PM members, along with the known members (each defined with a particular legend). We show the positions of these stars in the color–magnitude space in Figure 4. Our PM members located in the West and West-WFC3 fields are well within the RGB locus while the remaining two, located in Center-WFC3, are good RR Lyrae candidates. Our PM nonmembers help us to reduce heavy field contamination in the vicinity of the RGB. Stars with a color of ∼0.5 mag and magnitudes in the range 18.0 $\lesssim$ F814W $\lesssim$20.5 mag, extending above the HB level, were suggested to be variable stars (Adén

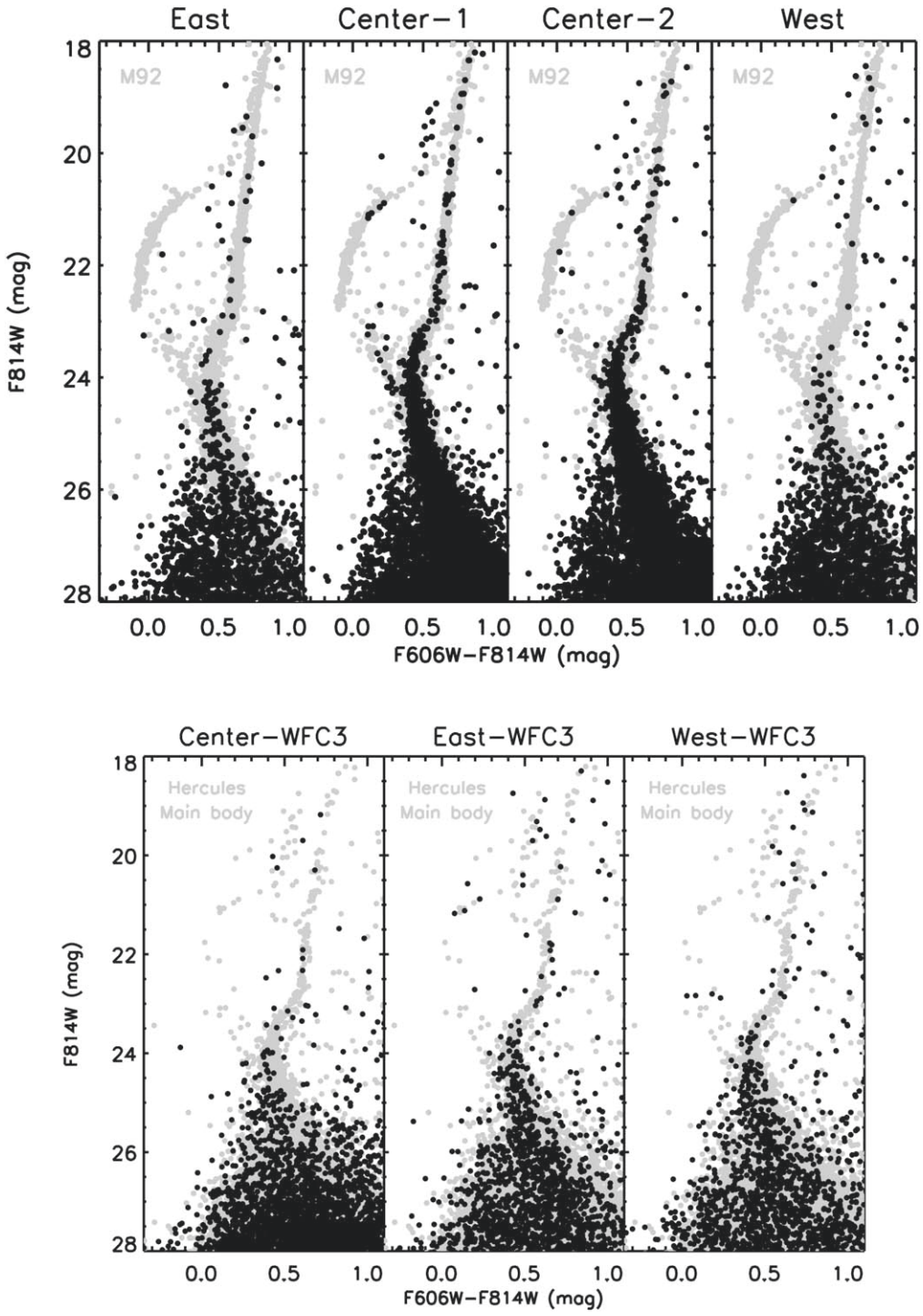

Figure 2. CMDs of our Hercules HST fields (black points). The top panel shows the ACS fields relative to M92 (gray points). The M92 stars are shifted to the distance modulus of Hercules ($m - M = 20.60$) from Sand et al. (2009), for comparison purposes; M92 displays a very close agreement with Hercules, providing an important empirical fiducial for ancient metal-poor stellar populations. The off-center fields reveal a clear main sequence, supporting the stellar extended structure seen in ground-based observations is genuine (Sand et al. 2009). The bottom panel shows a comparison of the CMDs of the Hercules WFC3 fields, relative to the Hercules main body (i.e., Center-1+Center-2) shown with gray points.

et al. 2009), however our Gaia investigation reveals that most are PM nonmembers and thus are not associated with Hercules.

In short, using the Gaia-DR2 data, we clean the literature spectroscopic samples from nonmembers and compile a set of robustly identified Hercules members while providing a new target list for further spectroscopic observations. We use this information to update the properties of Hercules (e.g., distance) and search for any signs of a distance gradient in this data.

5. Exploring the Distance Gradient across Hercules

Our goal is to explore whether or not Hercules presents a significant distance gradient across its projected length on the sky. We refer the reader to Figure 1 for our observational strategy. We also remind them that Center-1 and -2 are centered on the main body of Hercules while our other fields trace the outskirts of the galaxy. As shown in Section 3, M92 provides

Table 3
Structural Properties of Hercules

Parameter	Hercules	Reference
R.A. (h m s)	16: 31: 03.00	(1)
Decl. (d m s)	+12: 47: 13.77	(1)
M_V (mag)	-6.2 ± 0.4	(1)
r_h (arcmin)	5.91 ± 0.50	(1)
r_h (pc)	229.3 ± 19.4	(1)
Ellipticity	0.67 ± 0.03	(1)
Position angle (deg)	-72.36 ± 1.65	(1)
$m - M$ (mag)	20.58 ± 0.10	(2)
Distance (kpc)	130.6 ± 6.1	(2)
$\langle E(B-V) \rangle$	0.06	(2)
Heliocentric velocity (km s^{-1})	46.4 ± 1.3	(3)
Velocity dispersion (km s^{-1})	$4.4^{+1.4}_{-1.2}$	(3)
$\mu_\alpha \cos\delta$[a] (mas yr^{-1})	-0.153 ± 0.074	(3)
μ_δ[a] (mas yr^{-1})	-0.397 ± 0.063	(3)
Pericenter (kpc)	$50.9^{+24.2}_{-23.6}$	(3)
Apocenter (kpc)	$227.9^{+85.1}_{-38.1}$	(3)
Eccentricity	$0.65^{+0.10}_{-0.05}$	(3)

Notes. The references in the last column are as follows: (1) Sand et al. (2009), (2) this work, (3) Gregory et al. (2020).
[a] McConnachie & Venn (2020) recently found a very similar systemic proper motion for Hercules by examining simultaneously the likelihood of the spatial, color–magnitude, and proper-motion distribution of sources.

an important empirical fiducial for the stellar populations of Hercules, therefore the properties of Hercules can be robustly measured by making a comparison to the ridgeline of M92. Finally, we note that our HST fields reach a similar depth (see Table 1), hence they are comparable.

As a first test, we measure the distance modulus of each individual field with a simple chi-squared minimization routine based on the differences between the shape of the M92 fiducial and the observed sequences. We assume a distance modulus of $m - M = 14.62$ mag for M92 as in Brown et al. (2014), taking the mean of the measurements from Paust et al. (2007, 14.60 ± 0.09 mag), Del Principe et al. (2005, 14.62 ± 0.1 mag), and Sollima et al. (2006, 14.65 ± 0.1 mag). To reduce the contamination by foreground stars, we construct a selection region covering the RGB to SGB on our CMDs—stars brighter than 25.5 mag in F814W. First, we perform a CMD selection by including sources with colors and magnitudes expected for the stellar population of Hercules. A fairly broad selection is chosen here to ensure that we do not reject a significant fraction of the dwarf members. More specifically, we inflate the uncertainty to 0.05, 0.08, and 0.1 mag for F814W < 21, $21 \leqslant$ F814W < 24, F814W $\geqslant 24$ mag, respectively. Note that our photometric errors are much smaller than these floor uncertainties that we adopt. The selected stars are later cleaned of known nonmembers and stars whose Gaia proper motions are not consistent with those of the Hercules kinematic members (see Section 4). The final star catalogs used in our distance analysis are shown in Figure 5.

The M92 fiducial is shifted through 0.01 mag intervals in $(m - M)$ from 20.20 to 21.0 mag in F814W, a plausible range of distance moduli for Hercules. In each step, we calculate the chi-square statistic as

$$\chi^2 = \sum \frac{(c_{i,O} - c_{i,E})^2}{\sigma(c_{i,O})^2} \quad (1)$$

where $c_{i,O}$ is the observed color of the ith star, $c_{i,E}$ is the expected color of the same star on the fiducial at its magnitude, and $\sigma(c_{i,O})$ is its photometric uncertainty in color (based on our artificial star tests). In this step, we impose a floor photometric uncertainty of 0.005 mag, but we note that our true photometric uncertainties are smaller at F814W $\lesssim 22.0$ mag. We adopt the distance modulus that minimizes the chi-square statistic. Within our clean catalog, there might be stars associated with Hercules—either currently bound or in tidal material—and field stars. We use a 1000 iteration bootstrap analysis where the same number of stars are repeatedly drawn with replacement to determine the uncertainties due to the remaining contaminants. Especially for the off-center fields, where the number of stars is much smaller, the field star contamination might significantly affect distance measurements, and it is critical to properly take into account the known Hercules members in these poorly populated fields. Therefore, in each resampling, we purposely keep the known Hercules members and draw randomly from the remaining stars. From the 1000 realizations, we take the median as our final distance measurement and its standard deviation as our uncertainty.

We present the results of our bootstrap analysis in Figure 5, along with CMDs of our fields overlaid with the M92 fiducial at our derived distances. The bootstrap histograms of the central ACS fields are well-defined with an overlapping median at 20.58 mag and a small standard deviation ($\sim$0.02 mag). This translates to 130.6 ± 1.2 kpc, but the distance uncertainty here is only associated with the fit to our photometry, and do not include systematic errors associated with the M92 distance (the distance to M92 is uncertain at the level of $\lesssim$0.1 mag). When the systemic errors are included, the result becomes 130.6 ± 6.1 kpc, which is consistent with the distance estimates in the literature ranging from 132 ± 6 kpc to 147^{+8}_{-7} kpc (e.g., Belokurov et al. 2007; Coleman et al. 2007; Adén et al. 2009; Sand et al. 2009; Musella et al. 2012; Garling et al. 2018). In particular, our measurement is in perfect agreement with the distance estimations from RR Lyrae stars (132 ± 6 kpc, Musella et al. 2012; 137 ± 11 kpc, Garling et al. 2018). Since the off-center ACS fields are poorly populated, their histograms are broader, with a standard deviation of $\sim$0.1 mag. Intriguingly, the eastern bootstrap histogram has a median of $(m - M) = 20.46$ mag (123.6 kpc) while the western one peaks around $(m - M) = 20.71$ mag (138.7 kpc), implying a distance gradient of $\sim$0.25 mag ($\sim$15 kpc) across these off-center ACS fields. While this is interesting, the bootstrap histograms of the WFC3 fields (Figure 5, bottom-middle) have a significant overlap with an almost opposite trend (i.e., West-WFC3 seems to be slightly closer than East-WFC3 as its bootstrap histogram peaks at a lower distance modulus), casting doubt on the existence of a significant gradient. This is more clearly illustrated in the bottom right panel, which shows the distance modulus of each field as a function of the projected galactocentric distance. If the gradient is as strong as the ACS-only fields, then new intermediate ACS fields, which would have lower uncertainties, might provide significantly stronger constraints on the gradient.

To further explore the distance gradient, we fit a model with Hercules' distance changing linearly as a function of the major-axis distance, as previously done in Sand et al. (2009). This model assumes that Hercules is no longer a bound dwarf galaxy

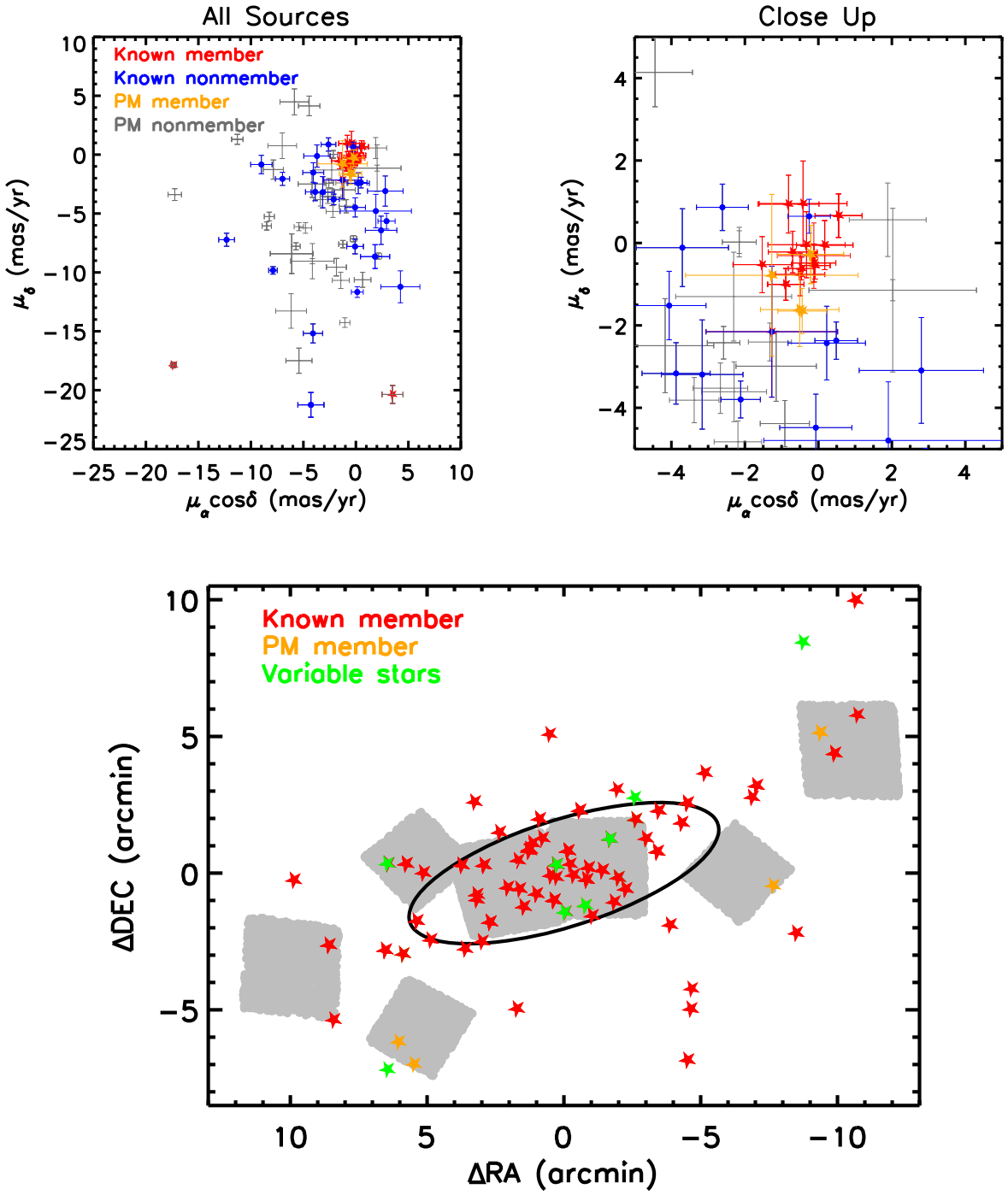

Figure 3. Top left: proper motions for all sources in our HST catalog with a match in Gaia DR2, including the known kinematic members (red) and nonmembers (blue) identified in Adén et al. (2009), Simon & Geha (2007), and Gregory et al. (2020). Top right: close-up of the stars with acceptable proper motions. We identify stars without spectroscopy but with a proper motion consistent with those of known members as PM members. Bottom: spatial distribution of the Hercules kinematic members (red), variable stars (green), and our four new possible members (i.e., PM members, orange). We highlight the positions of our HST pointings with gray fields, and the ellipse marks the nominal half-light radius of Hercules.

but instead a stellar overdensity in a thin stream whose length we are observing nearly along the line of sight. We adopt $(m - M) = 20.58$ mag (130.6 kpc) for the center of Hercules (see Figure 5), and then allow the observed-Hercules distance to change as a function of the major-axis distance:

$$\text{Distance}(x_i) = mx_i + 130.6\ (\text{kpc}). \quad (2)$$

For a given slope, m, and major-axis distance for the ith star, x_i, the presumed distance to a Hercules member is known, and the M92 fiducial is then transformed to that distance to interpolate the expected color. We choose to vary m between -2.5 and 3.6 kpc arcmin^{-1}, a plausible range of distance gradient for Hercules, with 0.05 kpc arcmin^{-1} intervals. We note that the slope proposed by Martin & Jin (2010) is -0.37 kpc arcmin^{-1}, which is well within the range we explore here. In each step, we calculate the chi-square statistic, as in Equation (1). The cartoon in Figure 6 illustrates our model, and the bottom panel

Table 4
A Clean Members Catalog for Hercules within Our HST Footprint

No	R.A. (deg)	Decl. (deg)	F606W (mag)	F814W (mag)	$\mu_\alpha \cos\delta$ (mas yr^{-1})	μ_δ (mas yr^{-1})	Field	Reference
1	247.80862	12.757386	19.17	18.34	-0.089 ± 0.410	-0.548 ± 0.328	Center-1	(1), (2)
2	247.78386	12.801684	19.17	18.34	-0.457 ± 0.362	-0.620 ± 0.276	Center-1	(1), (2), (6)
3	247.77063	12.785917	19.49	18.70	-0.885 ± 0.495	-1.004 ± 0.387	Center-1	(1)

Note. Column 1 lists our assigned number for each star. Columns 2–5 are the R.A., decl., and F606W and F814W magnitudes from our HST catalog (if they are within our fields), respectively. Columns 6 and 7 are the Gaia DR2 proper motions. Column 8 lists other IDs for each star from the literature. References are listed in Column 9: (1) Simon & Geha (2007), (2) Adén et al. (2009) (3) Deason et al. (2012), (4) Musella et al. (2012), (5) Garling et al. (2018), (6) Gregory et al. (2020).

(This table is available in its entirety in machine-readable form.)

Table 5
List of Plausible Hercules Members, Requiring Further Follow-up to Confirm

Field	R.A. (deg)	Decl. (deg)	F606W (mag)	F814W (mag)	$\mu_\alpha \cos\delta$ (mas yr^{-1})	μ_δ (mas yr^{-1})	CMD
West	247.60223	12.873091	20.09	19.36	-0.209 ± 0.899	-0.278 ± 0.708	RGB
West-WFC3	247.63171	12.779719	19.82	19.08	-0.441 ± 0.662	-1.652 ± 0.547	RGB
Center-WFC3	247.85607	12.67086	20.31	19.70	-0.508 ± 1.068	-1.616 ± 0.897	RRL
Center-WFC3	247.86572	12.684449	20.71	20.25	-1.266 ± 2.349	-0.784 ± 1.964	RRL

Note. Columns 1–5 are the field name, the R.A., decl., and F606W and F814W magnitudes from our HST photometry, respectively. Columns 6 and 7 are the Gaia DR2 proper motions. Column 8 reflects the position on the CMD.

(This table is available in machine-readable form.)

shows the results over 1500 bootstrap resamples. The bootstrap-derived histogram peaks at the slope of -0.10 kpc arcmin^{-1}, which is consistent with a zero or negligible slope, indicating no measurable distance gradient across the face of Hercules. However, the histogram is broad with a standard deviation of 0.48 kpc arcmin^{-1}, which still makes the Martin & Jin 2010 model plausible. We note that limiting the fitting to the magnitude interval around the turnoff (i.e., $22 < \mathrm{F814W} < 24.5$) yields results consistent within the uncertainties, and does not change our conclusion.

5.1. Simulated Data Sets

Before moving forward, we explore how well our method recovers the truth within the statistical uncertainty. We also want to better understand the limitations of our methodology. A natural step is to apply our two tests (one is deriving the distance for individual fields, the other is fitting a linearly changing distance model) on a series of artificial Hercules analogs with known distance gradients. We construct our model galaxy catalogs by sampling random stars from our M92 fiducial (after accounting for our photometric errors and adopting the observed luminosity function of Hercules), and placing stars using an exponential profile with the structural parameters (half-light radius $= 5\farcm9$, ellipticity $= 0.67$, position angle $= -72°$) in Table 3. We focus on four categories: (1) no distance gradient, (2) a slope of -0.10 kpc arcmin^{-1}, (3) the slope of the Martin & Jin 2010 model (i.e., -0.37 kpc arcmin^{-1}), and (4) a slope of -0.50 kpc arcmin^{-1}. Then, each star is shifted to the distance predicted by Equation (2). A total of 50 galaxies are generated in each category.

We utilize just the artificial stars located at the corresponding distances of our HST fields, treating these simulated star catalogs in the same way as our real data, and perform our tests as mentioned above. Overall, our first method is very successful at recovering the true mean distance of each individual field within the estimated uncertainties. However, in the cases of a significant distance gradient (Categories 3 and 4), we also find a number of simulated dwarf galaxies whose off-center fields show a flat or even opposite distance trend (just like in our WFC3 fields, see Figure 5-bottom). Similarly, it is possible to derive a strong gradient in some of the model galaxies with an intrinsically negligible distance gradient (Categories 1 and 2) due to "CMD shot noise" as described in Martin et al. (2008). A key point here is that the result must be taken with caution—while not finding a clear difference between the eastern and western portions of the galaxy reduces the likelihood of a real significant distance gradient, finding a flat trend between these sparsely populated off-center fields does not mean that Hercules has no distance gradient along the line of sight.

Next, we explore our star-by-star slope-fitting method on the simulated galaxies, and find that their bootstrap-derived histograms have a shape well represented by a Gaussian approximately centered on the true slope. Interestingly, these histograms are much narrower than the one we get for Hercules with an average scatter of $\sim$0.2 kpc arcmin^{-1} (see the green line in Figure 7). To explore the impact of field contamination, we use TRILEGAL, a simulator of photometry for stellar populations in the Galaxy (Girardi et al. 2012), and estimate the number of Galactic sources within the appropriate area. Considering that we already remove the nonmember stars while estimating the distance, we expect $\sim$2–6 more field stars per field. If we add field contamination to the model galaxies, their histograms become broader. However, their median might deviate from the true slope, as shown with an example Category 3 galaxy (with the slope of -0.37 kpc arcmin^{-1}, i.e., the Martin & Jin 2010 model), whose histogram peaks at -0.10 kpc arcmin^{-1} with a scatter of 0.40 kpc arcmin^{-1} in the presence of field contamination (see the red dashed–dotted

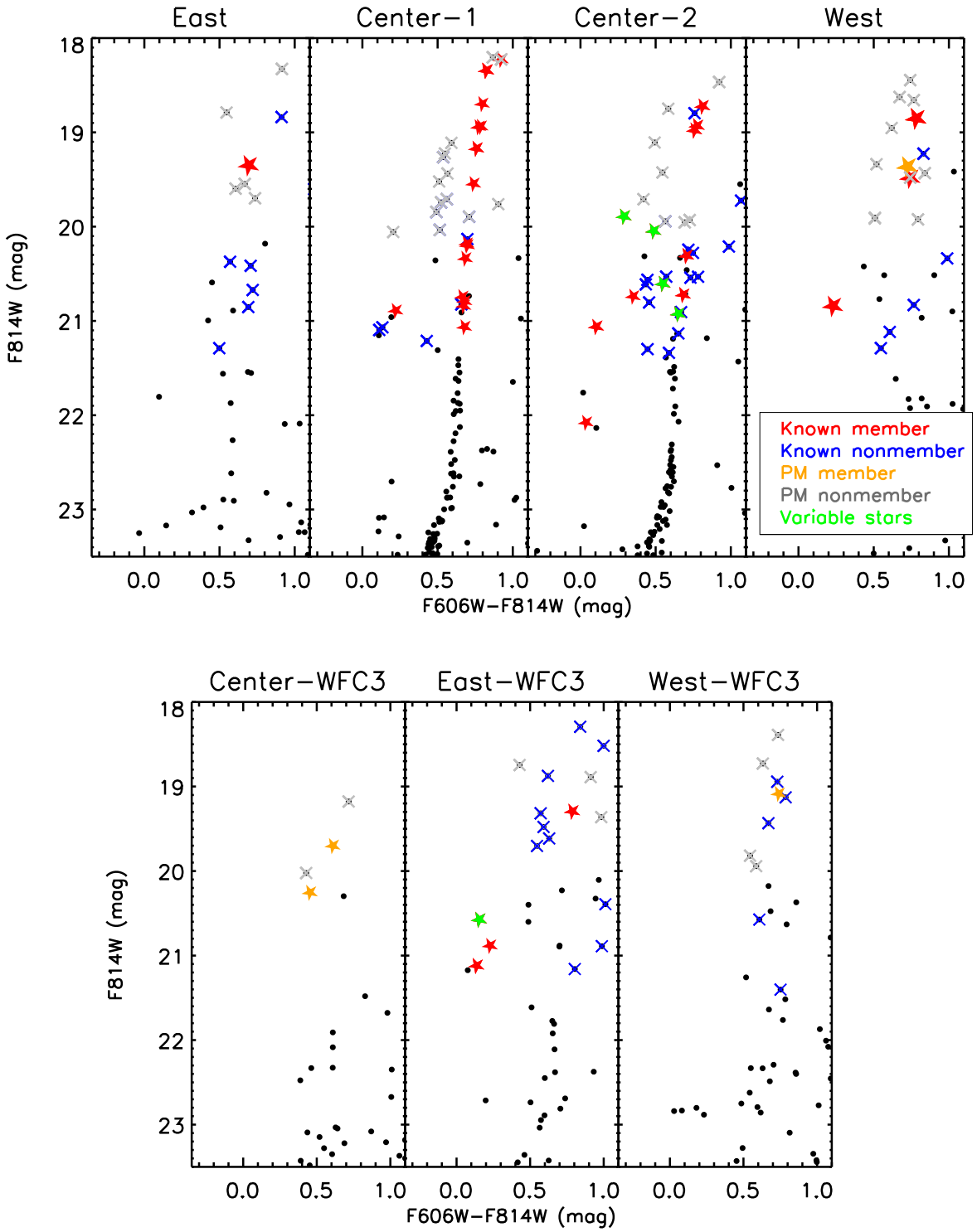

Figure 4. CMDs of our HST fields, highlighting the stars in Figure 3. Our proper-motion analysis allows us to disentangle a significant fraction of field contamination in the vicinity of the RGB (see PM nonmembers—gray crosses), while providing four new member candidates (see PM members—orange stars).

line). To better probe the complex nature of Hercules, we perform an additional test including an intrinsic thickness component to the stream, where each star is additionally shifted to a distance randomly sampled from a normal distribution with a standard deviation of ∼1 kpc (note that $r_h = 0.2$ kpc for Hercules, see Table 3). The thickness of a dwarf galaxy introduces additional uncertainty, and we find that on average the slope is overestimated half of the time. Overall, this means that constraining a distance gradient in such a faint system is not trivial, and the thickness of the dwarf and field contamination make it harder to distinguish between different models.

6. Conclusions

In this work, we present a comprehensive deep HST imaging study of Hercules and its surrounding regions, combined with Gaia DR2 archival data, and perform a new observational test

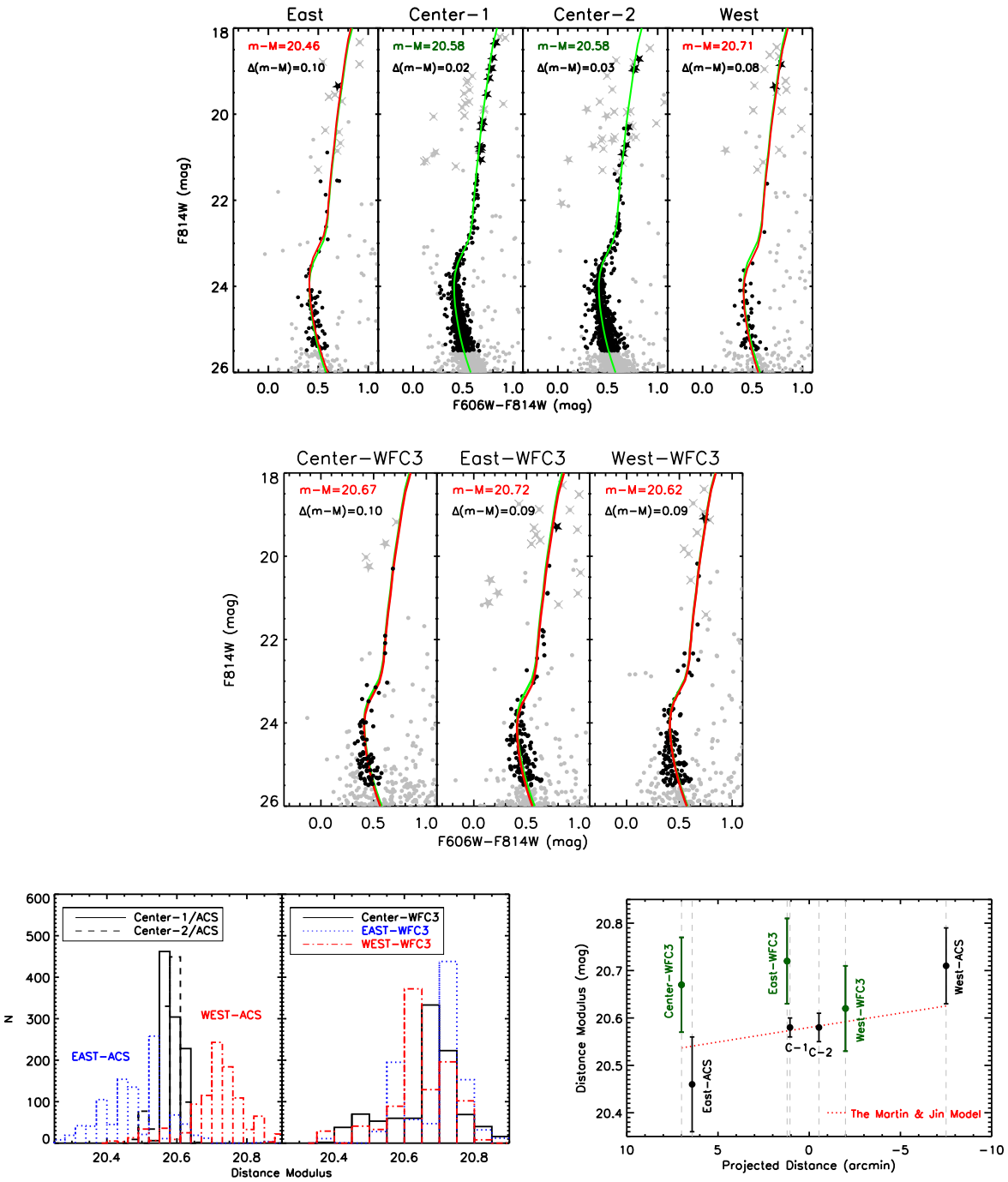

Figure 5. Top/middle: CMDs of the stars in our ACS/WFC3 fields (gray points), highlighting the ones used in our distance analysis (black points). Hercules' likely members—radial velocity and PM members—are shown as filled stars. Overplotted as a red line is the M92 fiducial at our derived distance for each individual field, and the green line refers to the one at $m - M = 20.58$ mag (the common value derived for the central two fields), shown for comparison purposes in all panels. $\Delta(m - M)$ is the uncertainty derived from our bootstrapping analysis. Bottom left/middle: bootstrap histograms of the distance modulus for our ACS/WFC3 fields. Bottom right: distance modulus vs. the projected distance of each field along the photometric major axis. For each field, we adopt the median of our bootstrap realizations as our final result, and use its standard deviation as our final uncertainty. Note that East-ACS seems to be closer (123.6 kpc) than West-ACS, however the WFC3 fields weaken this distance gradient argument.

for its orbital models by constraining the presence of a distance gradient in order to understand the peculiar properties of this ultrafaint system. Here, we summarize our key results:

1. For a better understanding of the properties of Hercules, we make a comparison with the Galactic globular cluster M92. The CMDs of the central Hercules fields display a close agreement with that of M92, implying they have similar stellar populations and star formation histories.
2. The CMDs of our off-center fields reveal a clear main sequence, supporting the idea that the stellar extension seen along the major axis of Hercules is real, not a clump of background galaxies (as found in Leo V, Mutlu-Pakdil et al. 2019).
3. As expected, our off-center fields are poorly populated and their RGBs suffer from significant field contamination. We utilize the Gaia DR2 proper-motion data to

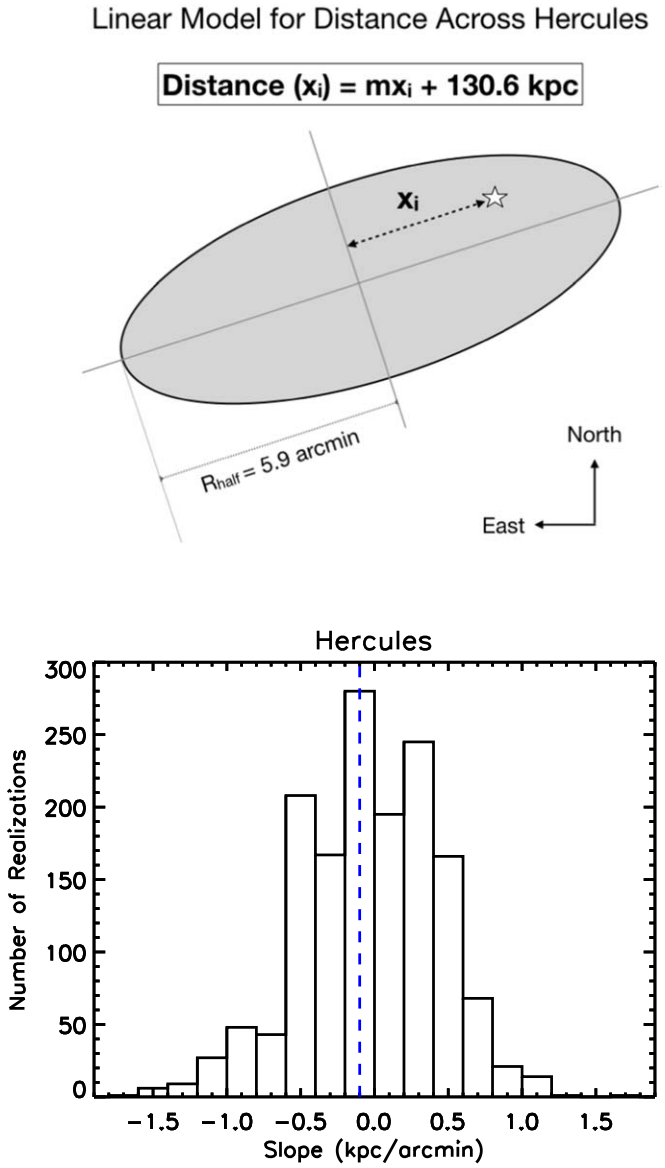

Figure 6. Top: illustration of our model for the observer–Hercules distance changing as a function of the major-axis distance. Bottom: histogram of the best-fitting slope with 1500 bootstrap resamples for which we fit our linearly changing distance model. The dashed line corresponds to the median, which is consistent with a zero or negligible slope.

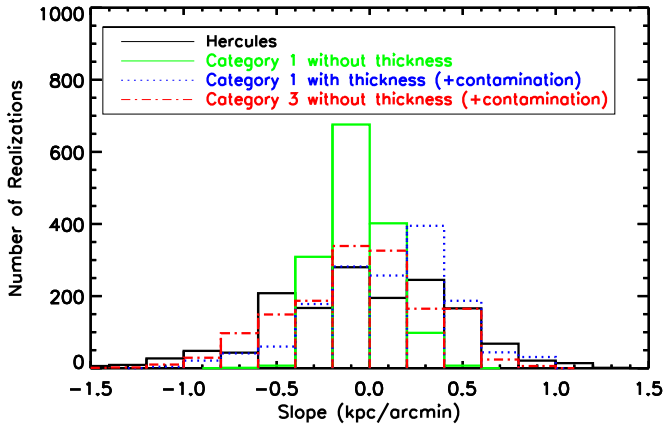

Figure 7. Histograms of the best-fitting slope for individual simulated dwarfs relative to that of Hercules. The green line shows an example Category 1 model galaxy (no distance slope; the estimated slope is -0.10 ± 0.18 kpc arcmin^{-1}). The other two examples include additional field contamination: the blue dotted line refers to an example Category 1 simulation with a thickness of $\sim$1 kpc (the estimated slope is 0.15 ± 0.37 kpc arcmin^{-1}), while the red dashed–dotted line shows an example Category 3 simulation (the Martin & Jin 2010 model) without an intrinsic thickness component (the estimated slope is -0.10 ± 0.40 kpc arcmin^{-1}). Note that we find a slope of -0.10 ± 0.48 kpc arcmin^{-1} for our real Hercules data. Both the thickness of the dwarf and field contamination introduce additional uncertainties, which makes it harder to distinguish between different models.

disentangle a significant fraction of field contaminants from Hercules members. We clean the literature spectroscopic samples from nonmembers (e.g., two previously identified spectroscopic members are now classified as PM nonmembers), compile a set of robustly identified Hercules members (see Table 4), and provide a new target list for further spectroscopic observations (i.e., two RGB and two RR Lyrae candidates which we classify as PM members, see Table 5).

4. We update the distance of Hercules with isochrone fitting, and find a distance of 130.6 ± 6.1 kpc ($m - M = 20.58 \pm 0.10$) for the main body, which is in excellent agreement with the distance measurements from RR Lyrae stars (132 ± 6 kpc, Musella et al. 2012; 137 ± 11 kpc, Garling et al. 2018).
5. Leveraging the $\sim 23'$ lever arm between our new ACS fields and coordinated parallel observations with WFC3, we probe the outskirts of the Hercules dwarf and attempt to constrain a predicted distance gradient across the face of Hercules, expected if Hercules is elongated from tides (Martin & Jin 2010). Fitting a linear gradient along the major axis of Hercules, we find the best fit model to our data is -0.10 ± 0.48 kpc arcmin^{-1}. This accuracy is insufficient to distinguish between competing models of Hercules, although the lack of a gradient is expected from Küpper et al. (2017).
6. Even with the deep HST imaging and Gaia proper-motion information, our work shows that constraining a distance gradient in such a faint system is not trivial, and the thickness of the dwarf and field contamination introduce additional uncertainties. Therefore, we advocate for combined studies (e.g., deep photometry, multi-epoch spectroscopy, astrometric data), with the aid of dedicated theoretical work, to understand the true nature of Milky Way UFDs.

Is Hercules a stellar stream in formation? It is hard to settle the question. Tidal destruction seems to be a viable option to explain its extreme ellipticity ($\sim$0.7) and observational evidence for association with a larger stream of stars (e.g., Adén et al. 2009; Sand et al. 2009; Deason et al. 2012; Roderick et al. 2015; Garling et al. 2018). On the other hand, Gregory et al. (2020) recently found no kinematic evidence in the form of a velocity gradient or velocity substructure. In this work, we address this problem with a complementary observational test, which is to search for a large distance gradient along its major axis, as proposed by Martin & Jin (2010). Given the large uncertainties, our findings do not constrain the orbital models of Hercules. On the other hand, since the models proposed by Küpper et al. (2017) and Martin & Jin (2010) are both slightly incompatible with the observed proper motions of Hercules (Gregory et al. 2020), alternative explanations for its elongated shape such as formation through mergers or puffy dispersion-dominated disks (e.g., Starkenburg

et al. 2016; Wheeler et al. 2017) should also be explored. Considering that the overdensities identified in Sand et al. (2009) are likely associated with Hercules, deep wide-area photometric follow-up studies in the era of the Rubin Observatory and the Roman Space Telescope can serve as one of the most powerful ways to identify stellar streams and constrain tidal stripping in UFDs. In addition to in depth observational studies, theoretical studies looking at the tidal distortion of UFDs are needed to understand the nature of UFDs and ultimately put them into context with respect to the cold dark matter paradigm for structure formation.

We are grateful to the referee for their constructive comments. This research is based on observations made with the NASA/ESA Hubble Space Telescope obtained from the Space Telescope Science Institute, which is operated by the Association of Universities for Research in Astronomy, Inc., under NASA contract NAS 5-26555. These observations are associated with program 15182. B.M.-P. is supported by an NSF Astronomy and Astrophysics Postdoctoral Fellowship under award AST-2001663. E.O. was partially supported by NSF grant AST1815767. J.S. acknowledges support from a Packard Fellowship.

Facilities: HST (ACS, WFC3), Gaia.

Software: The IDL Astronomy User's Library (Landsman 1993), DOLPHOT2.0 (Dolphin 2002), Topcat (Taylor 2005).

ORCID iDs

Burçin Mutlu-Pakdil https://orcid.org/0000-0001-9649-4815
David J. Sand https://orcid.org/0000-0003-4102-380X
Denija Crnojević https://orcid.org/0000-0002-1763-4128
Edward W. Olszewski https://orcid.org/0000-0002-7157-500X
Dennis Zaritsky https://orcid.org/0000-0002-5177-727X
Jay Strader https://orcid.org/0000-0002-1468-9668
Michelle L. Collins https://orcid.org/0000-0002-1693-3265
Anil C. Seth https://orcid.org/0000-0003-0248-5470
Beth Willman https://orcid.org/0000-0003-2892-9906

References

Adén, D., Wilkinson, M. I., Read, J. I., et al. 2009, ApJL, 706, L150
Bechtol, K., Drlica-Wagner, A., Balbinot, E., et al. 2015, ApJ, 807, 50
Behr, B. B. 2003, ApJS, 149, 67
Belokurov, V., Walker, M. G., Evans, N. W., et al. 2008, ApJL, 686, L83
Belokurov, V., Walker, M. G., Evans, N. W., et al. 2009, MNRAS, 397, 1748
Belokurov, V., Walker, M. G., Evans, N. W., et al. 2010, ApJL, 712, L103
Belokurov, V., Zucker, D. B., Evans, N. W., et al. 2007, ApJ, 654, 897
Brown, T. M., Tumlinson, J., Geha, M., et al. 2014, ApJ, 796, 91
Bullock, J. S., & Boylan-Kolchin, M. 2017, ARA&A, 55, 343
Carlin, J. L., & Sand, D. J. 2018, ApJ, 865, 7
Carretta, E., Bragaglia, A., Gratton, R., D'Orazi, V., & Lucatello, S. 2009, A&A, 508, 695
Coleman, M. G., de Jong, J. T. A., Martin, N. F., et al. 2007, ApJL, 668, L43
Deason, A. J., Belokurov, V., Evans, N. W., Watkins, L. L., & Fellhauer, M. 2012, MNRAS, 425, L101
Del Principe, M., Piersimoni, A. M., Bono, G., et al. 2005, AJ, 129, 2714
Dolphin, A. E. 2000, PASP, 112, 1383
Dolphin, A. E. 2002, MNRAS, 332, 91
Drlica-Wagner, A., Albert, A., Bechtol, K., et al. 2015, ApJL, 809, L4
Drlica-Wagner, A., Bechtol, K., Allam, S., et al. 2016, ApJL, 833, L5
Erkal, D., Li, T. S., Koposov, S. E., et al. 2018, MNRAS, 481, 3148
Fritz, T. K., Battaglia, G., Pawlowski, M. S., et al. 2018, A&A, 619, A103
Fu, S. W., Simon, J. D., & Alarcón Jara, A. G. 2019, ApJ, 883, 11
Garling, C., Willman, B., Sand, D. J., et al. 2018, ApJ, 852, 44
Girardi, L., Barbieri, M., Groenewegen, M. A. T., et al. 2012, ASSP, 26, 165
Gregory, A. L., Collins, M. L. M., Erkal, D., et al. 2020, MNRAS, 496, 1092
Homma, D., Chiba, M., Okamoto, S., et al. 2016, ApJ, 832, 21
Homma, D., Chiba, M., Okamoto, S., et al. 2018, PASJ, 70, S18
Ibata, R. A., Gilmore, G., & Irwin, M. J. 1994, Natur, 370, 194
Jin, S., & Martin, N. F. 2009, MNRAS, 400, L43
Kim, D., & Jerjen, H. 2015, ApJL, 808, L39
Kim, D., Jerjen, H., Mackey, D., Da Costa, G. S., & Milone, A. P. 2015, ApJL, 804, L44
King, J. R., Stephens, A., Boesgaard, A. M., & Deliyannis, C. 1998, AJ, 115, 666
Kirby, E. N., Boylan-Kolchin, M., Cohen, J. G., et al. 2013, ApJ, 770, 16
Kirby, E. N., Simon, J. D., Geha, M., Guhathakurta, P., & Frebel, A. 2008, ApJL, 685, L43
Koch, A., McWilliam, A., Grebel, E. K., Zucker, D. B., & Belokurov, V. 2008, ApJL, 688, L13
Koposov, S. E., Belokurov, V., Torrealba, G., & Evans, N. W. 2015, ApJ, 805, 130
Koposov, S. E., Walker, M. G., Belokurov, V., et al. 2018, MNRAS, 479, 5343
Küpper, A. H. W., Johnston, K. V., Mieske, S., Collins, M. L. M., & Tollerud, E. J. 2017, ApJ, 834, 112
Laevens, B. P. M., Martin, N. F., Bernard, E. J., et al. 2015a, ApJ, 813, 44
Laevens, B. P. M., Martin, N. F., Ibata, R. A., et al. 2015b, ApJL, 802, L18
Landsman, W. B. 1993, in ASP Conf. Ser. 52, Astronomical Data Analysis Software and Systems II, ed. R. J. Hanisch, R. J. V. Brissenden, & J. Barnes (San Francisco, CA: ASP), 246
Li, T. S., Simon, J. D., Kuehn, K., et al. 2018, ApJ, 866, 22
Longeard, N., Martin, N., Starkenburg, E., et al. 2018, MNRAS, 480, 2609
Martin, N. F., de Jong, J. T. A., & Rix, H.-W. 2008, ApJ, 684, 1075
Martin, N. F., & Jin, S. 2010, ApJ, 721, 1333
Martin, N. F., Nidever, D. L., Besla, G., et al. 2015, ApJL, 804, L5
Mau, S., Cerny, W., Pace, A. B., et al. 2020, ApJ, 890, 136
McConnachie, A. W., & Venn, K. A. 2020, AJ, 160, 124
Muñoz, R. R., Côté, P., Santana, F. A., et al. 2018, ApJ, 860, 66
Muñoz, R. R., Geha, M., & Willman, B. 2010, AJ, 140, 138
Musella, I., Ripepi, V., Marconi, M., et al. 2012, ApJ, 756, 121
Mutlu-Pakdil, B., Sand, D. J., Carlin, J. L., et al. 2018, ApJ, 863, 25
Mutlu-Pakdil, B., Sand, D. J., Walker, M. G., et al. 2019, ApJ, 885, 53
Okamoto, S., Arimoto, N., Yamada, Y., & Onodera, M. 2008, A&A, 487, 103
Paust, N. E. Q., Chaboyer, B., & Sarajedini, A. 2007, AJ, 133, 2787
Peterson, R. C., Kurucz, R. L., & Carney, B. W. 1990, ApJ, 350, 173
Roderick, T. A., Jerjen, H., Mackey, A. D., & Da Costa, G. S. 2015, ApJ, 804, 134
Roederer, I. U., & Sneden, C. 2011, AJ, 142, 22
Sand, D. J., Olszewski, E. W., Willman, B., et al. 2009, ApJ, 704, 898
Sand, D. J., Strader, J., Willman, B., et al. 2012, ApJ, 756, 79
Schlafly, E. F., & Finkbeiner, D. P. 2011, ApJ, 737, 103
Schlegel, D. J., Finkbeiner, D. P., & Davis, M. 1998, ApJ, 500, 525
Shipp, N., Drlica-Wagner, A., Balbinot, E., et al. 2018, ApJ, 862, 114
Simon, J. D. 2018, ApJ, 863, 89
Simon, J. D. 2019, ARA&A, 57, 375
Simon, J. D., & Geha, M. 2007, ApJ, 670, 313
Sneden, C., Pilachowski, C. A., & Kraft, R. P. 2000, AJ, 120, 1351
Sollima, A., Cacciari, C., & Valenti, E. 2006, MNRAS, 372, 1675
Starkenburg, T. K., Helmi, A., & Sales, L. V. 2016, A&A, 595, A56
Taylor, M. B. 2005, in ASP Conf. Ser. 347, Astronomical Data Analysis Software and Systems XIV, ed. P. Shopbell, M. Britton, & R. Ebert (San Francisco, CA: ASP), 29
Torrealba, G., Koposov, S. E., Belokurov, V., & Irwin, M. 2016, MNRAS, 459, 2370
Weisz, D. R., Dolphin, A. E., Skillman, E. D., et al. 2014, ApJ, 789, 148
Wheeler, C., Pace, A. B., Bullock, J. S., et al. 2017, MNRAS, 465, 2420